AD-A148 871 DEVELOPMENT OF A PROTOTYPE WAVEVECTOR-FREQUENCY SPECTRAL ANALYSIS SYSTEM(U) NAVAL UNDERWATER SYSTEMS CENTER NEW LONDON CT NEW LONDON LAB W A STRAWDERMAN

1/1

UNCLASSIFIED 12 DEC 84 NUSC-TD-7295 F/G 20/6 NL

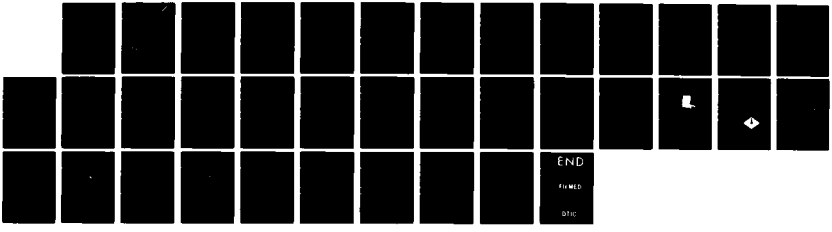

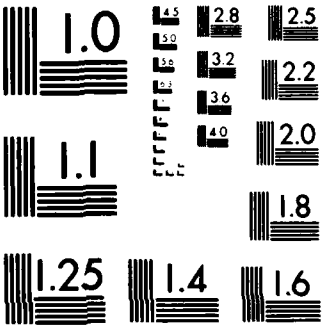

MICROCOPY RESOLUTION TEST CHART
NATIONAL BUREAU OF STANDARDS-1963-A

NUSC Technical Document 7295
12 December 1984

Development of a Prototype Wavevector-Frequency Spectral Analysis System

A Paper Presented at the 108th Meeting of the Acoustical Society of America, 8-12 October 1984, Minneapolis, Minnesota

Wayne A. Strawderman
Submarine Sonar Department

Naval Underwater Systems Center
Newport, Rhode Island / New London, Connecticut

PREFACE

This document was prepared under NUSC Project No. A12220, *External Array Development*, Principal Investigator Dr. H. H. Schloemer (Code 3233). The Sponsoring Activity was NAVSEA 63D, Program Manager J. Neely.

The preparation of the technical paper that forms the basis for this document was funded under NUSC Project No. A68011, *EEL Sensor Modeling*, Principal Investigator Dr. H. P. Bakewell (Code 3232). The Sponsoring Activity was NAVSEA 63R, Program Manager C. C. Walker.

The Technical Reviewer for this document was Dr. H. H. Schloemer.

REVIEWED AND APPROVED: 12 December 1984

F. J. Kingsbury

F. J. Kingsbury
Head, Submarine Sonar Department

The author of this document is located at the
New London Laboratory, Naval Underwater Systems Center,
New London, Connecticut 06320

REPORT DOCUMENTATION PAGE		READ INSTRUCTIONS BEFORE COMPLETING FORM
1. REPORT NUMBER TD 7295	2. GOVT ACCESSION NO. AD-A148 871	3. RECIPIENT'S CATALOG NUMBER
4. TITLE (and Subtitle) DEVELOPMENT OF A PROTOTYPE WAVEVECTOR-FREQUENCY SPECTRAL ANALYSIS SYSTEM		5. TYPE OF REPORT & PERIOD COVERED 6. PERFORMING ORG. REPORT NUMBER
7. AUTHOR(s) Wayne A. Strawderman		8. CONTRACT OR GRANT NUMBER(s)
9. PERFORMING ORGANIZATION NAME AND ADDRESS Naval Underwater Systems Center New London Laboratory New London, CT 06320		10. PROGRAM ELEMENT, PROJECT, TASK AREA & WORK UNIT NUMBERS
11. CONTROLLING OFFICE NAME AND ADDRESS Naval Sea Systems Command Washington, DC 20362		12. REPORT DATE 12 December 1984 13. NUMBER OF PAGES 30
14. MONITORING AGENCY NAME & ADDRESS(if different from Controlling Office)		15. SECURITY CLASS. (of this report) UNCLASSIFIED 15a. DECLASSIFICATION/DOWNGRADING SCHEDULE

16. DISTRIBUTION STATEMENT (of this Report)

Approved for public release; distribution unlimited.

17. DISTRIBUTION STATEMENT (of the abstract entered in Block 20, if different from Report)

18. SUPPLEMENTARY NOTES

19. KEY WORDS (Continue on reverse side if necessary and identify by block number)

Array Development	Spectral Analysis System
Diagnostic Tools	Structural-Acoustic Analyses
Prototype Systems	Wavevector
Sampling, Spatial and Temporal	Wavevector-Frequency Spectrum

20. ABSTRACT (Continue on reverse side if necessary and identify by block number)

This document consists of the text and slides of an invited paper presented at the 108th Meeting of the Acoustical Society of America, held in Minneapolis, Minnesota, from 8 to 12 October 1984. The following abstract was published in the program for the 108th Meeting (J. Acoust. Soc. Am., Supplement 1, Vol. 76, Fall 1984).

By the mid-1970's, the use of wavevector-frequency spectral analysis as a diagnostic tool for structural-acoustics had been theoretically and-

20. (Cont'd)

experimentally demonstrated. In anticipation of a continuing need for this diagnostic capability, we decided to develop a wavevector-frequency spectral analysis system suitable for general application in spatially planar fields. This paper outlines the development of that prototype system, from theory to hardware. Emphasis is focused on the practical aspects of the development and the consequences of design decisions. Data from a simple, but practical, application of the system are presented and discussed.

DEVELOPMENT OF A PROTOTYPE WAVEVECTOR-FREQUENCY SPECTRAL ANALYSIS SYSTEM

INTRODUCTION

In 1977, we decided to develop a wavevector-frequency spectral analysis system suitable for general application in spatially planar fields. This paper describes the development of that system and illustrates some of its capabilities and limitations.

Slide 1

DEVELOPMENT OF A PROTOTYPE WAVEVECTOR-FREQUENCY SPECTRAL ANALYSIS SYSTEM

TOPICAL OUTLINE

- THEORY OF WAVEVECTOR-FREQUENCY SPECTRAL ESTIMATION
- TRANSLATION OF THEORY TO HARDWARE
- EXAMPLES OF SYSTEM CAPABILITIES

As indicated in this slide, the paper is organized in three sections: the first section outlines the theoretical basis for our system design; the second section describes the practical problems of translating the theory to hardware; and the third section presents some examples of wavevector spectral data that were obtained during acceptance tests of the system.

THEORETICAL BASIS

DEFINITIONS

Slide 2

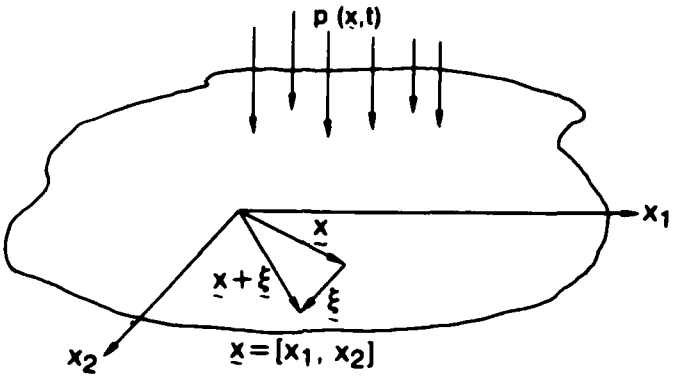

SPACE-TIME CORRELATION OF THE PRESSURE FIELD (Q_{pp})

$$Q_{pp}(\underline{x}, \underline{\xi}, t, \tau) = E\left\{ p(\underline{x}, t)\, p(\underline{x}+\underline{\xi}, t+\tau) \right\}$$

STATIONARY FIELD (CORRELATION INDEPENDENT OF ABSOLUTE TIME, t)

$$Q_{pp}(\underline{x}, \underline{\xi}, t, \tau) = Q_{pp}(\underline{x}, \underline{\xi}, \tau)$$

HOMOGENEOUS FIELD (CORRELATION INDEPENDENT OF ABSOLUTE SPATIAL POSITION, $\underline{x}$)

$$Q_{pp}(\underline{x}, \underline{\xi}, t, \tau) = Q_{pp}(\underline{\xi}, t, \tau)$$

HOMOGENEOUS AND STATIONARY FIELD (CORRELATION INDEPENDENT OF $\underline{x}$ AND t)

$$Q_{pp}(\underline{x}, \underline{\xi}, t, \tau) = Q_{pp}(\underline{\xi}, \tau)$$

The field illustrated at the top of this slide is the pressure at the surface of the plane defined by the x_1 and x_2 axes. Although we use pressure to illustrate the planar field, the field could just as well be acceleration, stress, or another quantity of interest.

The correlation of the pressure field over the plane of interest is defined as the average value, over many observations, of the product of (1) the pressure at the vector location $\underline{x}$ and time t and (2) the pressure at vector location $\underline{x} + \underline{\xi}$ and time $t + \tau$. The average value is denoted by capital E.

In general, the correlation is a function of (1) the absolute spatial position and the time of one observation of the pressure and (2) the spatial separation vector and the time difference between observations. A stationary field is one in which the correlation and all other statistical moments are independent of the absolute time of observation, t, and depend only on the time between observations, τ. Similarly, a homogeneous field is one in which the correlation is independent of absolute spatial position ($\underline{x}$) and depends only on the spatial separation vector ($\underline{\xi}$) between observations.

In diagnostic testing, we can usually control the temporal nature of system excitation so that, for practical purposes, the field of interest is stationary.

Homogeneity is another matter. The pressure field associated with a plane wave propagating through a homogeneous medium is a homogeneous field. On the other hand, the pressure field near a vibrating, rib–stiffened plate is nonhomogeneous, owing to the space–varying impedance of the plate. Both of these fields are of practical interest in acoustics.

Because we felt we could control the temporal aspects of the excitation in diagnostic situations, we limited our attention to stationary fields. However, we decided that, as a general diagnostic tool, the system should be capable of analyzing both homogeneous and nonhomogeneous fields.

Slide 3

DEFINITIONS OF WAVEVECTOR-FREQUENCY SPECTRA

STATIONARY HOMOGENEOUS FIELD

$$\Phi_p^H(\underset{\sim}{k}, \omega) = \frac{1}{(2\pi)^{3/2}} \iint_{-\infty}^{\infty} Q_{pp}(\underset{\sim}{\xi}, \tau)\, e^{-i(\underset{\sim}{k}\cdot\underset{\sim}{\xi} + \omega\tau)}\, d\underset{\sim}{\xi} d\tau$$

WAVEVECTOR $\underset{\sim}{k} = [k_1, k_2]$; CIRCULAR FREQUENCY $\omega = 2\pi f$

STATIONARY NONHOMOGENEOUS FIELD

SPACE-VARYING SPECTRUM (K_p)

$$K_p(\underset{\sim}{x}, \underset{\sim}{k}, \omega) = \frac{1}{(2\pi)^{3/2}} \iint_{-\infty}^{\infty} Q_{pp}(\underset{\sim}{x}, \underset{\sim}{\xi}, \tau)\, e^{-i(\underset{\sim}{k}\cdot\underset{\sim}{\xi} + \omega\tau)}\, d\underset{\sim}{\xi} d\tau$$

SPACE-AVERAGED SPECTRUM (Φ_p)

$$\Phi_p(\underset{\sim}{k}, \omega; A) = \frac{1}{A} \int_A K_p(\underset{\sim}{x}, \underset{\sim}{k}, \omega)\, d\underset{\sim}{x}$$

TWO-WAVEVECTOR SPECTRUM ($\mathcal{Z}_p$)

$$\mathcal{Z}_p(\underset{\sim}{\mu}, \underset{\sim}{k}, \omega) = \frac{1}{2\pi} \int_{-\infty}^{\infty} K_p(\underset{\sim}{x}, \underset{\sim}{k}, \omega)\, e^{-i\underset{\sim}{\mu}\cdot\underset{\sim}{x}}\, d\underset{\sim}{x}$$

$\underset{\sim}{\mu} = [\mu_1, \mu_2]$

The wavevector–frequency spectrum is defined by Fourier transformation of the space–time correlation on the spatial separation vector $\underset{\sim}{\xi}$ and the time difference τ.

This transformation is defined for the stationary homogeneous field at the top of the slide. Here, Φ_p is the wavevector–frequency spectrum and the superscript H designates the homogeneous field.

The wavevector $\underset{\sim}{k}$ is the Fourier conjugate variable of the spatial separation vector $\underset{\sim}{\xi}$, and the circular frequency ω is the conjugate variable of the time difference τ.

For the nonhomogeneous field, three different wavevector-frequency spectra can be defined. The space-varying spectrum K_p uses the same transformation as the homogeneous field, but because the correlation is a function of the absolute spatial vector $\underset{\sim}{x}$, this wavevector-frequency spectrum also varies with $\underset{\sim}{x}$.

The space-averaged spectrum Φ_p is simply the average value of the space-varying spectrum over some area, A, in absolute space.

The two-wavevector-frequency spectrum $\mathcal{K}_p$ introduces a second wavevector, $\underset{\sim}{\mu}$, by an additional spatial Fourier transformation. The second wavevector is the conjugate variable of the absolute spatial vector $\underset{\sim}{x}$.

We based our general purpose system on the space-averaged spectrum. This choice was made for two reasons. First, for a homogeneous field, the space-averaged spectrum reduces to the definition of the spectrum for a homogeneous field, and, therefore, this spectral form accommodates both homogeneous and nonhomogeneous fields. Second, the space-averaged form leads to the simplest computational algorithm for estimating the wavevector-frequency spectrum.

SAMPLING AND THE ALGORITHM

The definition of the space-averaged spectrum assumes knowledge of the field over all space and time. In practice, we can only obtain a sampling of the field over some finite region of space and time.

Slide 4

SPATIAL SAMPLING

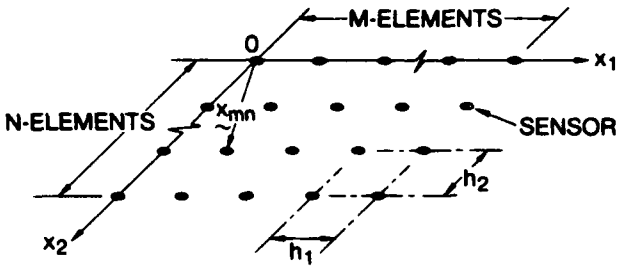

OUTPUT VOLTAGE OF THE mn^{TH} SENSOR

$$e(\underset{\sim}{x}_{mn}, t) = S\, p(\underset{\sim}{x}_{mn}, t)$$

TEMPORAL SAMPLING

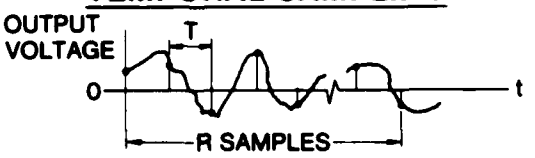

AVAILABLE DATA

$$e(mh_1, nh_2, rT) = S\,\eta(mh_1, nh_2)\,\rho(rT)\,p(mh_1, nh_2, rT); \quad \begin{matrix} 0 \le m \le M-1 \\ 0 \le n \le N-1 \\ 0 \le r \le R-1 \end{matrix}$$

OUTPUT VOLTAGE | SENSITIVITY | SPATIAL WEIGHTING | TEMPORAL WEIGHTING | PRESSURE

For our system, we decided that spatial sampling of the field by a rectangular array of sensors, similar to that shown at the top of this slide, would offer the most flexibility.

Each sensor converts the pressure over its active surface to a voltage, e. We assume that the sensors are small compared to any wavelength of interest and, for practical purposes, respond instantaneously in time. Therefore, the output voltage of each sensor is related to the local pressure by a constant sensitivity, S.

From the outset, we intended that the spectral analysis would be performed by digital techniques. This requires that a series of time samples, spaced T seconds apart, be taken simultaneously from the outputs of all sensors of the array. The temporal sampling of the output voltage of a sensor is illustrated in the middle of this slide.

If we provide for spatial weighting, η, of the array and temporal weighting, ρ, of the output voltage samples to reduce the sidelobe responses associated with the spatial and temporal sampling, the available data are the discrete set of output voltage samples shown at the bottom of this slide. These data are the input to an algorithm that estimates the wavevector–frequency spectrum.

Slide 5

THE ALGORITHM:

$$\hat{\Phi}_e(\underline{k}, \omega) = \frac{h_1 h_2 T}{(2\pi)^{3/2} MNRJ} \sum_{j=1}^{J} \left| E_j(\underline{k}, \omega) \right|^2,$$

WHERE

$$E_j(\underline{k}, \omega) = \sum_{m=0}^{M-1} \sum_{n=0}^{N-1} \sum_{r=0}^{R-1} e_j(mh_1, nh_2, rT) \exp\left[-i(k_1 mh_1 + k_2 nh_2 + \omega rT)\right]$$

AND

j DENOTES THE SAMPLES FROM THE j^{TH} MEMBER OF THE ENSEMBLE.

RELATION BETWEEN ESTIMATED AND TRUE SPECTRA FOR HOMOGENEOUS FIELD:

$$\underbrace{E\left\{\hat{\Phi}_e(\underline{k}, \omega)\right\}}_{\text{MEAN VALUE OF ESTIMATED VOLTAGE SPECTRUM}} = \frac{h_1 h_2 TS^2}{(2\pi)^3 MNR} \int\int_{-\infty}^{\infty} \underbrace{\Phi_p^H(\underline{\gamma}, \Omega)}_{\text{TRUE PRESSURE SPECTRUM}} \underbrace{\left|H(\underline{\gamma} - \underline{k})\right|^2}_{\text{WAVEVECTOR RESPONSE OF ARRAY}} \underbrace{\left|\mathcal{R}(\Omega - \omega)\right|^2}_{\text{FREQUENCY RESPONSE OF TIME SAMPLING PROCESS}} d\underline{\gamma} d\Omega.$$

THE WAVEVECTOR RESPONSE OF THE ARRAY IS

$$H(\underline{k}) = \sum_{m=1}^{M} \sum_{n=1}^{N} \eta(mh_1, nh_2) \exp\left[-i(k_1 mh_1 + k_2 nh_2)\right].$$

THE FREQUENCY RESPONSE ASSOCIATED WITH THE TIME SAMPLING IS

$$\mathcal{R}(\omega) = \sum_{r=1}^{R} \rho(rT) \exp\left[-i\omega rT\right].$$

The computational algorithm is shown at the top of this slide. The estimate of the space-averaged spectrum (denoted by $\hat{\Phi}_e$) is seen to be proportional to the squared magnitude of the discrete Fourier transform (in wavevector and frequency) of the output voltage samples.

Because the field is sampled over a limited portion of space and time, the algorithm provides only an estimate of the wavevector-frequency spectrum. The relationship between the mean of this spectral estimate and the true wavevector-frequency spectrum for a homogeneous pressure field is shown below the algorithm. A similar, but more complex, relationship exists for the nonhomogeneous field.

For the homogeneous field, the mean of the wavevector-frequ estimate is proportional to the convolution of the true wavevector-frequ of the pressure field of interest with the squared magnitudes of (1) th response of the array used to spatially sample the field and (2) the frequ associated with the temporal sampling. The wavevector response of the a the discrete wavenumber transform of the spatial weighting applied Similarly, the frequency response associated with the temporal sampling i frequency transform of the weighting applied to the temporal samples. squared magnitudes of both the wavevector response and the frequency periodic functions.

The wavevector response of the array and the frequency respons sampling process control the quality of the spectral estimate. Therefore, necessary to examine the impact of these functions on the design of system.

Slide 6

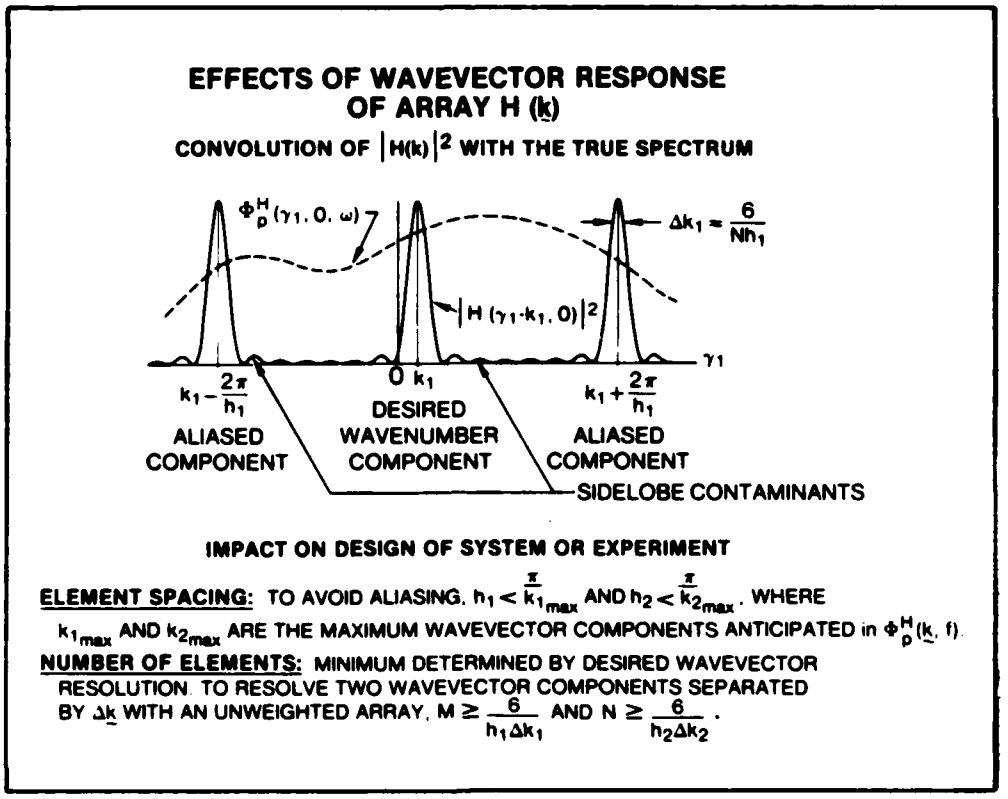

The convolution of the wavevector response of the array with the true wavevector–frequency spectrum is illustrated for a fixed frequency at the top of this slide. Here, the array is steered to sample the true spectrum at the wavenumber k_1. However, because of the periodic nature of the array wavevector response, we see that the true spectrum is also sampled at the wavenumbers corresponding to the periodic replicates of the main response lobe. In the convolution process, the samples at these periodic replicates are added to the sample at k_1, thereby contaminating the estimate of the spectrum at k_1. This contamination is called aliasing.

A similar, but usually lower order, contamination results from the sampling of the true spectrum by the sidelobes of the array response.

To get a good estimate of the true wavevector spectrum, we must avoid aliasing, minimize sidelobe contamination, and minimize the main lobe width of the array response function.

Aliasing is avoided by selection of the interelement spacings of the array such that the periodic replicates of the main response lobe occur at wavenumbers twice as large as any anticipated wavevector component of the true spectrum. This constraint is listed near the bottom of the slide, where we can see that the wider the wavevector content of the true spectrum is, the smaller the interelement spacing of the array must be.

Sidelobe contamination is controlled by the appropriate choice of the spatial weighting applied to the array.

The width of the main lobe of the array response function is inversely proportional to the overall dimensions of the array. Therefore, to achieve a narrow main lobe, we need a large array. With the interelement spacing set to avoid aliasing, narrowing of the main lobe must be accomplished by increasing the number of elements in the array. Because there is a practical limit to the number of elements we can afford and/or process, it is desirable to establish some lower limit on the number of array elements. This minimum is based on the wavevector resolution that we require from the array. The resolution requirement is listed at the bottom of the slide for an unweighted array and states that the closer the two wavevector components that we wish to resolve are, the greater the number of elements we require.

Slide 7

EFFECTS OF TEMPORAL SAMPLING

CONVOLUTION OF $|\mathcal{R}(f)^2|$ WITH FILTERED TRUE SPECTRUM

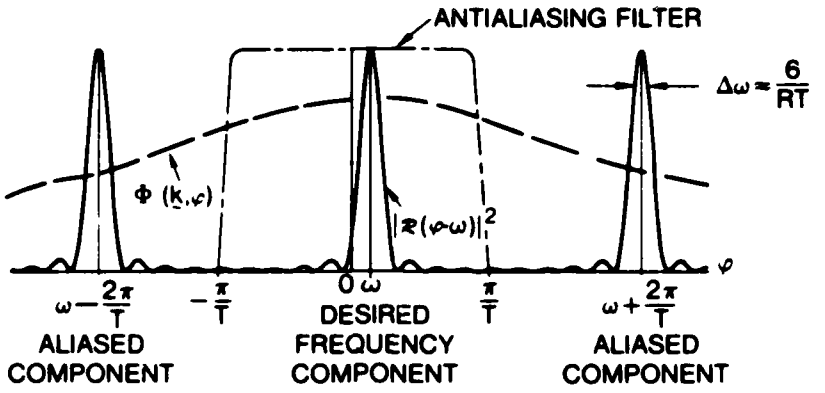

IMPACT ON DESIGN OF SYSTEM OR EXPERIMENT

ANTIALIASING FILTERS: USED TO LIMIT FREQUENCY CONTENT OF TRUE SPECTRUM.

SAMPLING FREQUENCY ($2\pi/T$): TO AVOID ALIASING, THE SAMPLING FREQUENCY MUST BE AT LEAST TWICE THE CUTOFF FREQUENCY (ω_{max}) OF THE ANTIALIASING FILTER, OR $(2\pi/T) \geq 2\omega_{max}$.

NUMBER OF SAMPLES (R): MINIMUM DETERMINED BY DESIRED FREQUENCY RESOLUTION. FOR UNWEIGHTED TEMPORAL SAMPLING, THE FREQUENCY RESOLUTION, $\Delta\omega$, IS ABOUT 6/RT.

The convolution of the frequency response associated with the temporal sampling with the true spectrum is illustrated at the top of this slide. Here we see the same potential for aliasing and sidelobe contamination effects in frequency that we saw in wavenumber in the previous slide. However, in temporal sampling of data, it is common practice to low-pass filter the signal prior to digitization to limit the frequency content of the signal to some desired range. (Unfortunately, we do not yet have effective antialiasing filters in the wavevector domain.) To avoid contamination due to aliasing, we only require that the temporal sampling frequency be greater than twice the cutoff frequency of the filter.

The number of temporal samples required in each observation is then dictated by the frequency bandwidths in which we wish to analyze the data; the narrower the bandwidth, the more samples are required.

In this and the preceding slide, it should be clear that the quality of the wavevector-frequency spectral estimate depends on our ability to achieve the desired wavevector filter characteristics by the array design and the desired frequency filter characteristics in the temporal sampling. From a design viewpoint, desired filter characteristics translate into large numbers of sensors, high sampling rates, and large numbers of temporal samples.

TRANSLATION OF THEORY TO HARDWARE

Slide 8

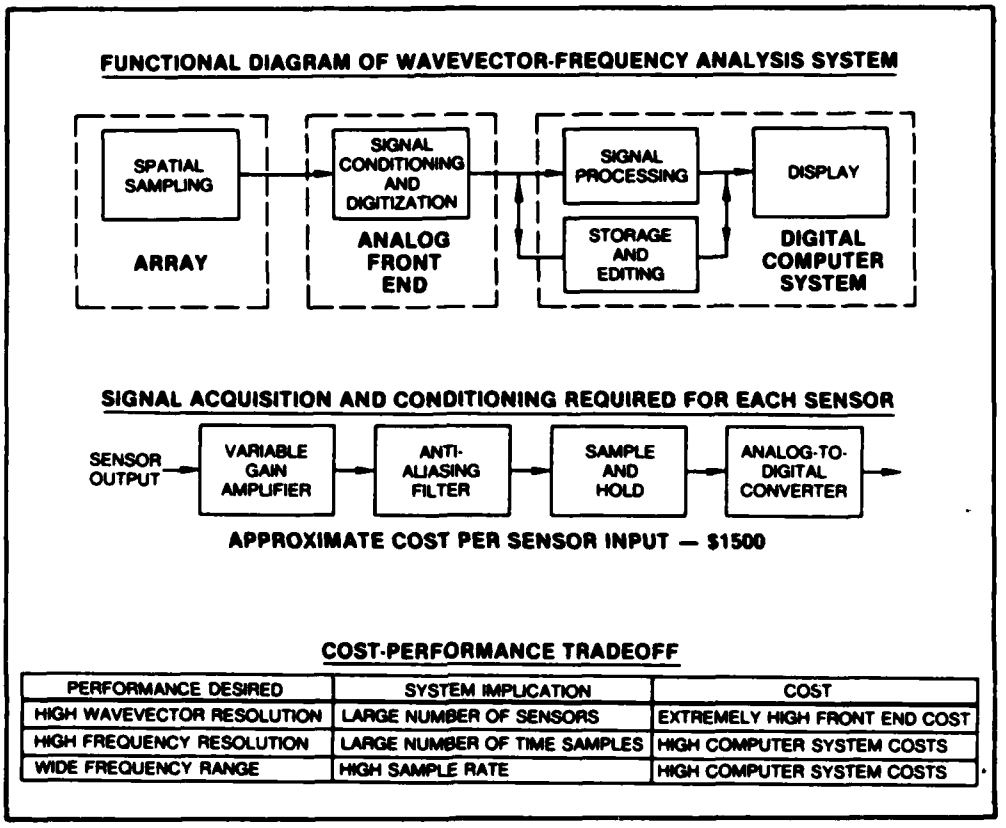

COST-PERFORMANCE TRADEOFF

PERFORMANCE DESIRED	SYSTEM IMPLICATION	COST
HIGH WAVEVECTOR RESOLUTION	LARGE NUMBER OF SENSORS	EXTREMELY HIGH FRONT END COST
HIGH FREQUENCY RESOLUTION	LARGE NUMBER OF TIME SAMPLES	HIGH COMPUTER SYSTEM COSTS
WIDE FREQUENCY RANGE	HIGH SAMPLE RATE	HIGH COMPUTER SYSTEM COSTS

The functional elements required to implement the spectral estimation algorithm are illustrated at the top of this slide. The field of interest is sampled by an array of sensors. The time varying output of each sensor is then appropriately gained, filtered, and converted to a digital format.

The discrete space-time samples of the field are Fourier transformed and converted to a wavevector-frequency spectral estimate by the appropriate signal processing. The display unit provides the graphic output of the spectral estimates.

A mass storage medium is required for editing of the data and permanent storage of the spectral estimates.

The functional elements of the system can be accommodated in three physical components. These components (indicated by the dashed lines in the functional diagram) are an array of sensors, an analog front end, and a digital computer system.

The analog front end deserves special attention. The components required to condition and digitize the signal from a single sensor are shown in the middle of the slide. The signal from each sensor must first be amplified to take maximum advantage of the dynamic range of the analog-to-digital converter. The signal is then low-pass filtered to control aliasing, sampled in time, and converted to digital format.

To maintain dynamic range in the wavevector response of the array, the amplifiers and filters must be closely matched between sensors. To our surprise and dismay, the cost of the close-matched, antialiasing filters alone was about $1000 per channel, resulting in a front-end cost of nearly $1500 per channel.

A cursory examination of the cost-performance tradeoffs of this system concept is shown at the bottom of the slide. The bottom line is that high wavevector resolution increases front-end costs and high frequency resolution increases computer system costs.

Slide 9

COST ESTIMATES FOR MINIMAL SYSTEM

DEFINITION OF MINIMAL SYSTEM

FREQUENCY RANGE — 0-5 kHz
FREQUENCY RESOLUTION — 5 Hz
ARRAY SIZE — 36 ELEMENTS [6 × 6 GRID]
ARRAY GEOMETRY — RECTANGULAR

INPUT DATA RATE OF MINIMAL SYSTEM

INPUT DATA RATE = SAMPLE RATE × NUMBER OF ARRAY ELEMENTS
≈ 450,000 WORDS/S

COST ESTIMATES (1977)

FRONT END COST	$ 48K
COMPUTER SYSTEM COST	
OPTION 1: REAL TIME PROCESSING	>$200K
OPTION 2: NONREAL TIME PROCESSING	$100K
APPROX. TOTAL	$150-250K
PROTOTYPE SYSTEM BUDGET	$100K

This slide shows the estimated cost of a minimal system. The minimal system accommodates outputs from 36 elements arranged in a 6 by 6 grid and provides wavevector–frequency spectral estimates in 5–Hz bands over the frequency range of 0 to 5 kHz.

For a sampling frequency that is 2 1/2 times the upper frequency of interest, the front end generates digital data at the rate of 450,000 words per second. As indicated in the center of the slide, this is the rate at which data are input into the digital

computer. The computer must either process these data at the rate at which they are input -- that is, in real time -- or store all or a portion of the data for later processing.

To process the data in real time, the computer must be able to perform five three-dimensional discrete Fourier transforms each second. In 1977, such computational power was available only in the more expensive computers.

If we choose not to process the data in real time, such computational speed is not required, and a moderately priced computer can be used. However, the input data rate is about three times higher than the rate at which data can be transferred to disc. This means that most of the data must be stored in bulk memory. In 1977, such a bulk memory capability cost approximately $50,000.

The cost estimate for the basic system is shown at the bottom of this slide. Here, in addition to the front-end cost, we estimated the cost for both real and nonreal time processing. The nonreal time system, costing about $150,000, was the least expensive; however, it was approximately $50,000 over our budget of $100,000.

Slide 10

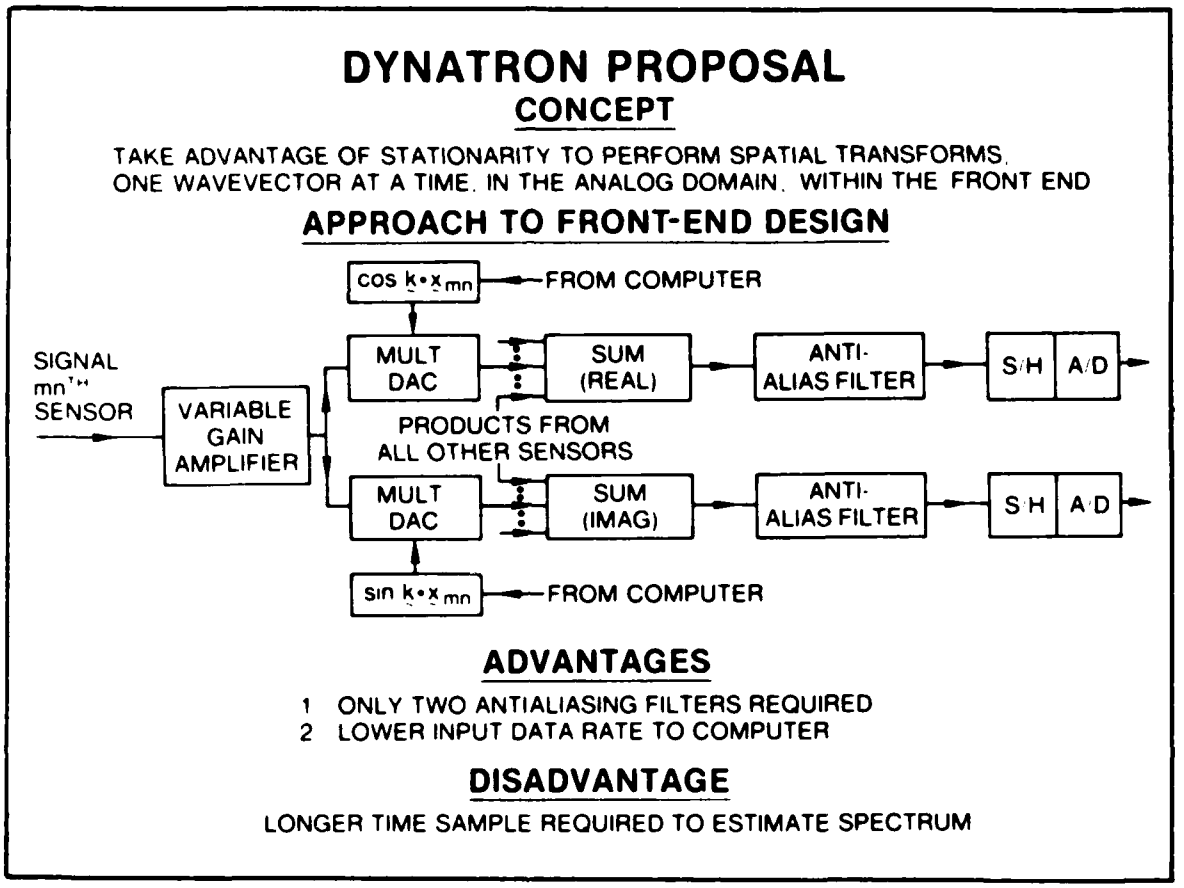

Our dilemma was resolved by a novel approach proposed by Dynatron Corporation of Waltham, Massachusetts. Dynatron's concept was to take advantage of the stationary nature of the signals by performing the spatial transform in the analog domain, one wavevector at a time, within the front end.

Dynatron's approach to the front-end design is illustrated for a typical sensor output in the center of the slide. Here, the signal from the mn^{th} sensor is first amplified. Then, by means of multiplying digital-to-analog converters (labeled DAC's in the slide), the signal is separately multiplied by the cosine and sine of the scalar product of the wavevector of interest and the vector location of the sensor. The cosine and sine values are stored in the computer system and are supplied to the DAC's by a data link. This multiplication process is applied to each sensor in the array. The products of each signal with the appropriate cosine term are then summed to form the

real part of the discrete spatial transform. A similar summation of the terms involving the sine forms the imaginary part of the spatial transform. Both real and imaginary parts are continuous functions of time.

The real and imaginary components are then separately low-pass filtered, temporally sampled, digitized, and stored in the computer system. When sufficient temporal samples have been gathered, the computer changes the coefficients applied to the multiplying DAC's to those that are appropriate for the next wavevector in a predetermined sequence, and the process is repeated.

When temporal samples have been collected for all wavevector values in the sequence, the temporal transformation is performed in the digital computer, and an estimate of the wavevector-frequency spectrum is formed. Stability of the estimate is accomplished by multiple repetition of the estimation process and averaging of the spectral estimates.

The Dynatron approach offers two distinct advantages over our previous approach. The first is that only two signals are output at any time from the front end, and, therefore, only two antialiasing filters are required. Therefore, the Dynatron approach results in substantially lower front-end costs. (Multiplying DAC's are inexpensive components.)

The second advantage is that the input data rate to the computer is only twice the temporal sampling rate. At this input rate, the data can easily be transferred to disc or tape. Thus, the requirement for large bulk storage in the computer system is eliminated, substantially reducing computer system costs.

The Dynatron approach has one distinct disadvantage. That is, since the spatial transform is performed in the front end, one wavevector at a time, the time required to collect sufficient data for a single spectral estimate is relatively long.

Dynatron estimated that they could design and build the minimal system within our budget, and they were funded to do this.

Slide 11

ONLINE WAVEVECTOR-FREQUENCY ANALYSIS SYSTEM

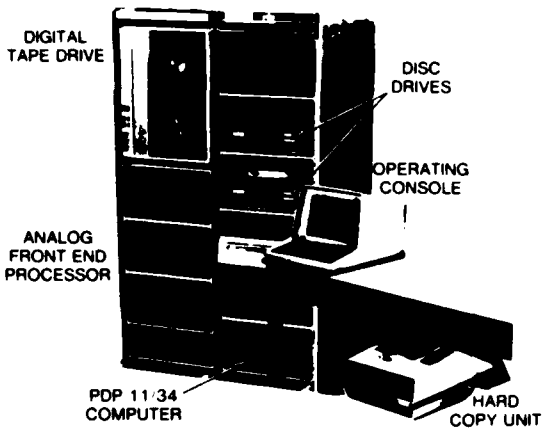

SYSTEM CAPABILITY

ARRAY INPUT CAPACITY	36 ELEMENTS (6 X 6 GRID)
ARRAY GEOMETRY	RECTANGULAR
FREQUENCY RANGE	FOUR OPERATOR-SELECTED BANDS — 0-2000 Hz, 0-4000 Hz, 0-6000 Hz, 0-8000 Hz
FREQUENCY RESOLUTION	1 25 Hz, 2 5 Hz, 3 75 Hz, 5 Hz

The system delivered by Dynatron is shown in this slide. It consists of the analog front-end processor with input capacity for a 6 by 6 element array. The frequency transformation and spectral estimate are performed by a PDP 11/34 computer. Two disc drives provide storage for system software and data files. Intermediate data and final spectral estimates are stored on digital tape. The system is operated through a console, and printed output is obtained by means of a hard copy unit.

As shown at the bottom of the slide, the system has four operator-selected frequency ranges, with upper frequency limits of 2000, 4000, 6000, and 8000 Hz. A 4096-point temporal transform is used in all frequency ranges, so that the frequency resolution varies from approximately 1.25 Hz in the 2000-Hz range to approximately 5-Hz in the 8000-Hz range. The input gain is operator selected between 0 and 60 dB in 10-dB increments.

EXAMPLES OF SYSTEM CAPABILITIES

After receiving the system, we performed a series of acceptance tests; the results from two of these tests will be used to illustrate some of the system capabilities.

The first test was a zero-wavevector calibration of the system for a square array. The zero wavevector was simulated by applying a common signal synchronously to all input channels of the system. The wavevector spectral estimate for the zero-wavevector input is equal to the squared magnitude of the wavevector response of an unshaded 6 by 6 element array.

The next slides illustrate three of the ouput formats of the system for the zero-wavevector calibration.

Slide 12

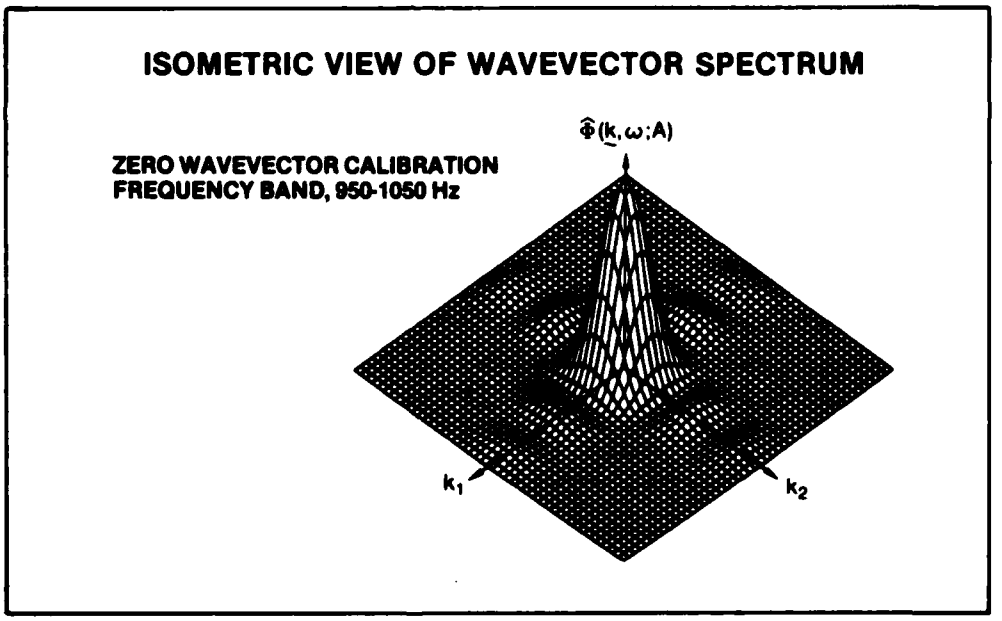

This slide shows a three-dimensional isometric view of the wavevector spectral estimate in a 100-Hz band that is centered around 1 kHz. Here, all scales are linear, and the shape of the spectral estimate is consistent with the two-dimensional sin Nx over sin x behavior expected for the wavenumber response of a square, unshaded array.

Slide 13

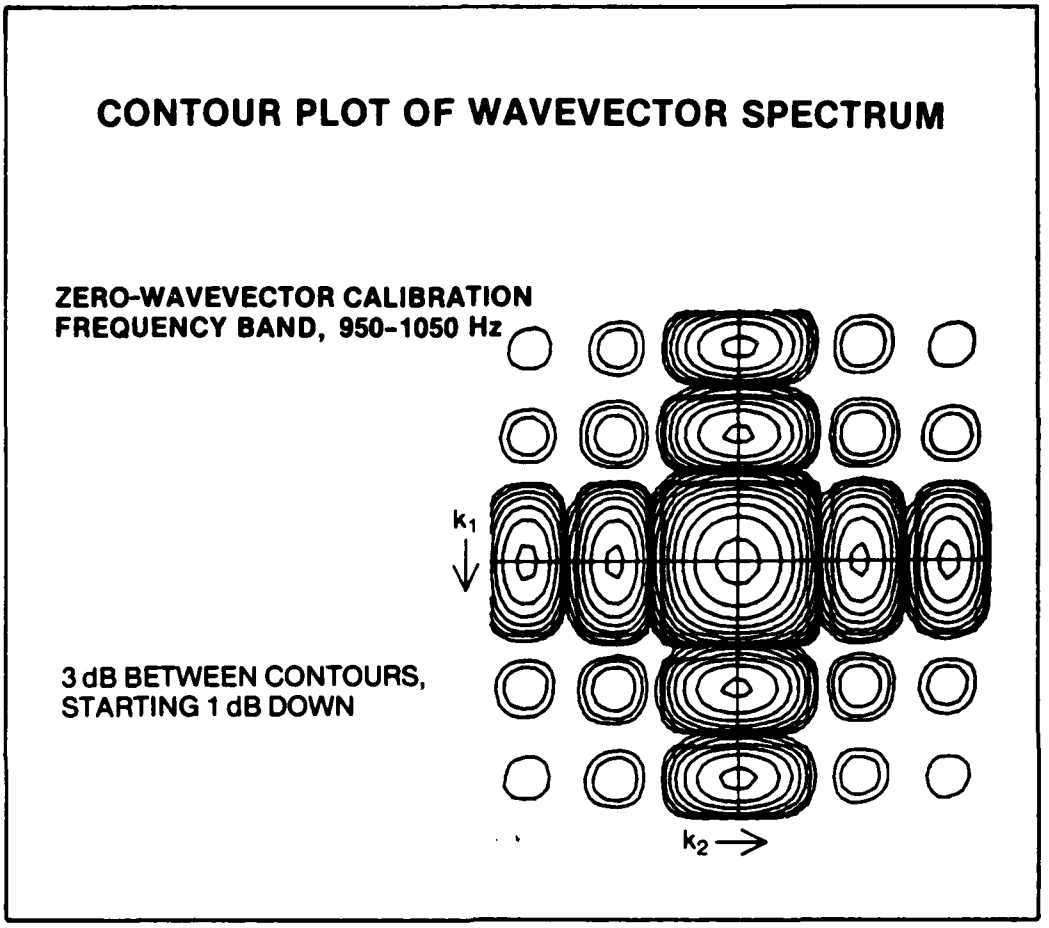

This slide shows the same spectral estimate as the previous slide in the form of a contour plot. This format more clearly illustrates the main and sidelobe pattern of the array response. In the contour plot format, the number of contours, the difference (in decibels) between contours, and the difference (in decibels) between the spectral maximum and the first contour are operator selected.

LISTING OF WAVEVECTOR SPECTRAL M/

ZERO-WAVEVECTOR CALIBRATION
FREQUENCY BAND, 950-1050 Hz

MAXIMUM	K1	K2	K
0.230E−01	0.0000	0.0000	0.0(
0.133E−02	0.0000	0.4301	0.4
0.132E−02	0.0000	−0.4301	0.4
0.131E−02	0.4301	0.0000	0.4
0.131E−02	−0.4301	0.0000	0.4
0.689E−03	0.7480	0.0000	0.7
0.687E−03	0.0000	0.7480	0.7
0.685E−03	−0.7480	0.0000	0.7
0.679E−03	0.0000	−0.7480	0.7
0.768E−04	−0.4301	0.4301	0.6(
0.768E−04	0.4301	−0.4301	0.6(
0.708E−04	−0.4301	−0.4301	0.6(

The third output format is a listing of the maxima of the waveve and the wavevectors corresponding to each maximum within the freq interest. The last column, labeled K, is the magnitude of the wavevec with the maximum. The spectral maxima are presented on a linear sca input voltage. For the zero–wavevector calibration data shown h maximum is the zero–wavevector spectral density, and subsequent maxi to sidelobes of the wavevector response of the array.

The interelement spacing of the array in this zero–wavevector c assumed to be 3.5 inches, and the wavevector locations of the sidelob choice.

Slide 15

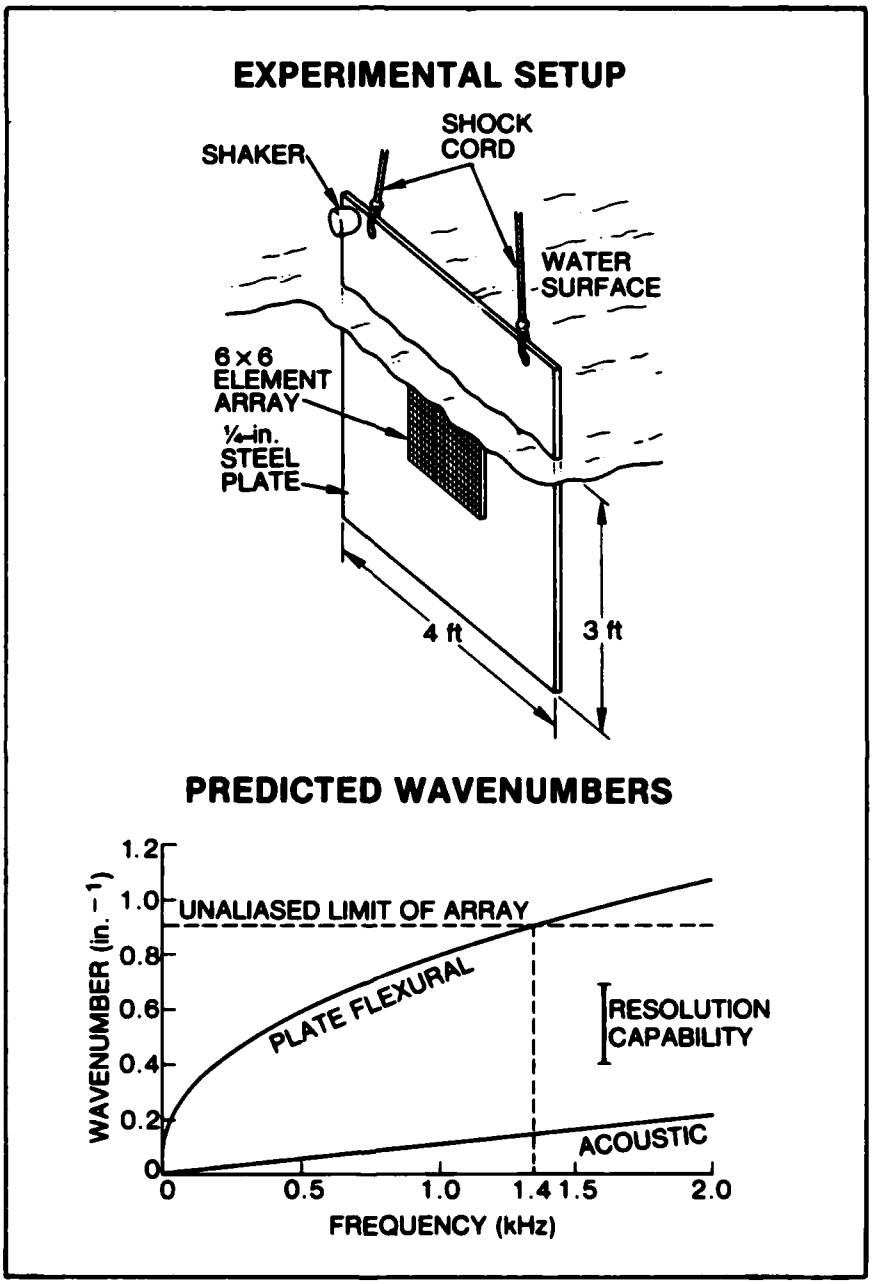

One of the acceptance tests more closely simulated the use of the system as a diagnostic tool. This test is illustrated at the top of the slide. Here, a 6 by 6 element array of hydrophones is attached to one face of a 4-foot-square section of 1/4-inch steel plate. The plate is suspended by shock cord so that 3 feet of the plate is

in water. The plate is excited into vibration by a shaker mounted above the water surface. We want to measure the wavevector-frequency characteristics of the pressure in the nearfield of this vibrating plate.

A general idea of the wavenumber-frequency characteristics of the nearfield noise can be obtained if we consider the physical mechanisms by which the energy from the shaker is transferred to the water near the plate.

The shaker excites flexural vibrations in the plate, which, in turn, produce a nearfield pressure component. This nearfield component is characterized by the wavenumber associated with flexural waves in the fluid-loaded plate. The predicted magnitude of the flexural wavenumbers of the fluid-loaded 1/4-inch steel plate is shown as a function of frequency in the lower portion of the slide.

The flexural waves are scattered at the plate boundaries, giving rise to pressure waves that propagate through the water at the speed of sound. Because the plate edges are the apparent source of such waves, these scattered acoustic waves propagate over the surface of the array at sonic velocities. The magnitude of the wavevectors associated with these acoustic components is also shown in the lower portion of the slide.

The array used in this test was an unshaded, square array with interelement spacings of 3.5 inches. Based on our previous arguments, the spectral estimate from this array will be unaliased only for wavevector components less than π divided by the interelement spacing, or wavenumbers less than approximately nine-tenths of a reciprocal inch. As shown in the slide, this means that the wavevector spectral estimate will be contaminated by aliased flexural wave components above 1400 Hz. Consequently, the random noise excitation to the shaker was low-pass filtered to 1400-Hz.

With the limited aperture of this array, the wavevector resolution is approximately three-tenths of a reciprocal inch, as shown on the right-hand side of the wavenumber-frequency plot. Such poor resolution means that we cannot resolve flexural and acoustic waves below 100 Hz or two grazing acoustic waves traveling in opposite directions at frequencies below 1350 Hz.

Slide 16

CONTOUR PLOT OF WAVEVECTOR SPECTRUM

FREQUENCY BAND, 1034–1041 Hz

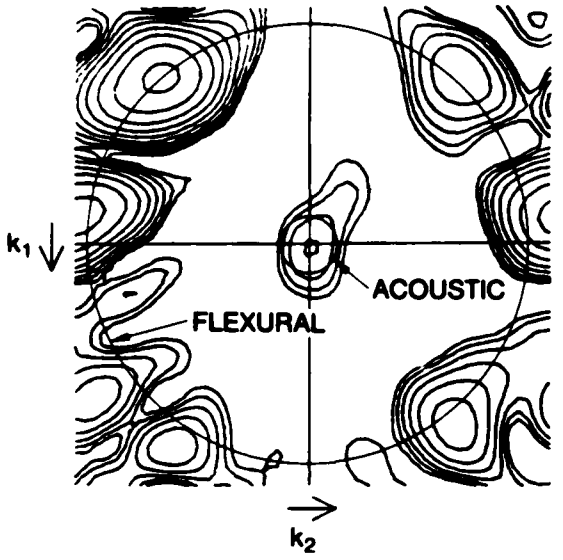

This is a contour plot of the wavevector spectrum of the nearfield pressure of the plate in the 7-Hz band between 1034 and 1041 Hz. Superimposed on the contour plot are two circles, with radii equal to the wavenumbers predicted for flexural waves in the fluid-loaded plate and for grazing incidence acoustic waves at the midband frequency of 1037 Hz.

Note that the majority of the wavevector spectral peaks fall on or near the circle characterizing flexural waves of the plate. These wavevector components of the nearfield pressure can therefore be presumed to be caused by the local coupling of the vibration field of the plate to the water.

The wavevector spectral peak near the origin, which is about 12 dB lower than the largest spectral peak at the upper left, is clearly not a single grazing incidence acoustic component because it does not lie on the predicted acoustic circle. Rather, owing to the inability of the array to resolve multiple acoustic wavevector contributions at frequencies less than 1350 Hz, it is probable that this spectral peak results from two or more grazing acoustic contributions. We say "probable" because the level of this spectral peak is too high to result from a combination of off-axis sidelobes, and the location of the peak does not coincide with an on-axis sidelobe of any of the major spectral peaks.

In any case, the level of this spectral contribution in the acoustic region is small in comparison with those contributions associated with flexural waves in the plate.

Slide 17

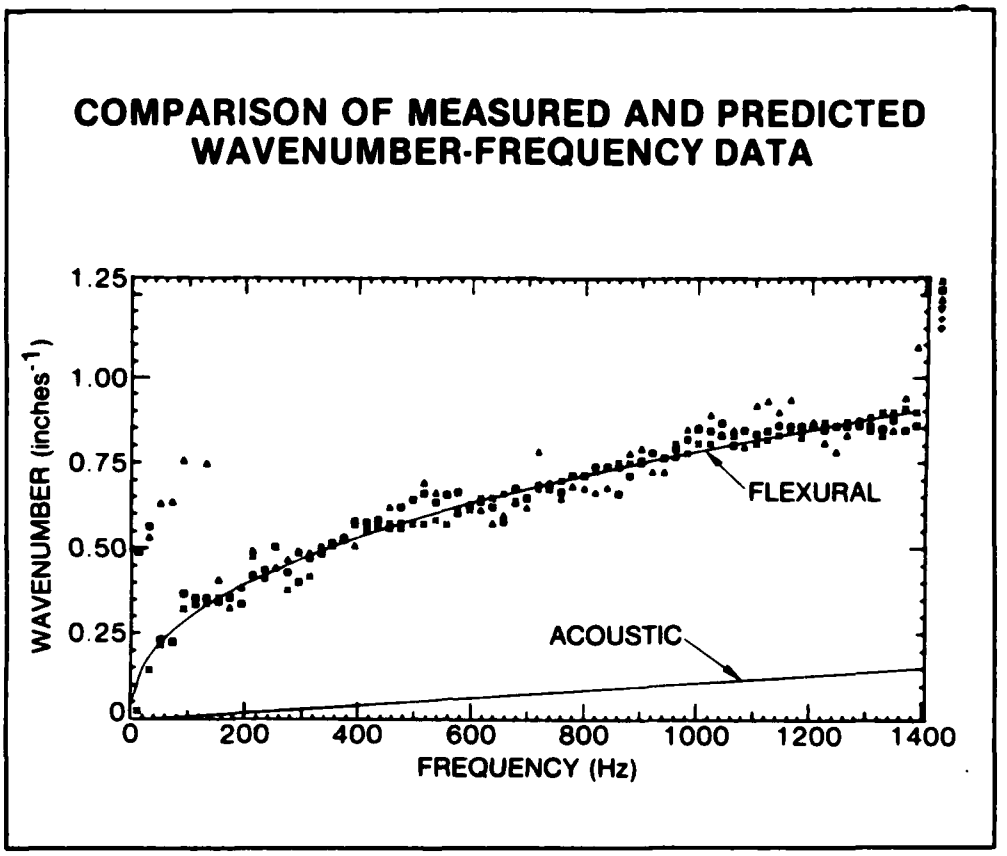

This slide illustrates another output format of the system. Here, the magnitudes of the wavevectors associated with the three largest wavevector spectral contributions to the nearfield pressure of the plate in each 20-Hz band between 0 and 1400 Hz are plotted as a function of frequency. For comparison, the predictions of the flexural wavenumber of the fluid-loaded plate and the wavenumber associated with grazing incidence acoustic waves are superimposed on the measured data.

The data show that the three largest wavevector contributions to the pressure in the nearfield of the plate, in each 20-Hz band above 120 Hz, occur at wavevectors consistent, in magnitude, with flexural waves in the 1/4-inch plate. No wavevector

spectral contributions are shown in the acoustic wavenumber range. The scattering of wavenumbers above the flexural wavenumber of the plate at low frequencies can be traced to sidelobes of the flexural wavevector component.

Based on these data, it is evident that the pressure in the nearfield of the vibrating plate is dominated by wavevector components associated with flexural vibrations of the plate. The data also show that the edge-scattered acoustic waves do not appear to contribute significantly to the nearfield pressure.

This slide illustrates, quite well, the utility of the wavenumber-frequency plot as a diagnostic tool.

Slide 18

SUMMARY

- WE HAVE DEVELOPED A PROTOTYPE SYSTEM FOR GENERAL PURPOSE WAVEVECTOR-FREQUENCY SPECTRAL ANALYSIS.
- PRINCIPAL LIMITATIONS OF SYSTEM ARE
  1) LIMITED WAVEVECTOR RESOLUTION DUE TO INPUT CAPACITY FOR 36 ELEMENT ARRAY.
  2) RELATIVELY LONG PROCESSING TIME.
- PROTOTYPE SYSTEM HAS BECOME A PRINCIPAL DIAGNOSTIC TOOL FOR ANALYSIS OF STRUCTURAL-ACOUSTIC FIELDS.

In summary, we have developed a prototype system for general purpose wavevector–frequency spectral analysis of spatially planar fields. The system has only two shortcomings of consequence:

(1) limited wavevector resolution, which results from the 36–channel input limitation of the system and

(2) the relatively long time record required to form a spectral estimate.

Despite these limitations, the system has proved to be a useful diagnostic tool and has been in near continuous use over the past 6 years for the analyses of a variety of structural–acoustic fields.

INITIAL DISTRIBUTION LIST

Addressee	No. of Copies
ONR (ONR-220 (T. J. Warfield))	1
DIA	1
NRL (Dr. J. Hansen, Dr. R. Menton)	2
NRL, USRD (Dr. L. Van Buren)	1
NAVSEASYSCOM (SEA-63D, -63R-1 (C. Walker))	2
NOSC (Library, Code 6565)	1
DWTNSRDC BETH (Code U31, -U31 (Dr. G. Maidanik, E. F. Geib))	3
NAVPGSCOL	1
ARL/PENN STATE, STATE COLLEGE (Dr. Sabih Hayek)	1
DTIC	12
MAR, INC. (Dr. L. King)	1
BBN (Dr. N. C. Martin, Dr. K. L. Chandiramani)	2
FLORIDA ATLANTIC UNIV. (Dr. J. M. Cuschieri)	1
VIBRASOUND RESEARCH CORP. (Dr. G. F. Kuhn)	1
PURDUE UNIV. (Dr. J. S. Bolton)	1
DYNATRON CORP. (R. Zaorski)	1

END

FILMED

2-85

DTIC